applied sciences

MDPI

Article

Assessment of the Structural State of Dissimilar Welded Joints by the Acoustic Emission Method

Vera Barat [1,*], Artem Marchenkov [1], Vladimir Bardakov [1,2], Daria Zhgut [1], Marina Karpova [1], Timofey Balandin [1] and Sergey Elizarov [2]

[1] Moscow Power Engineering Institute, National Research University, 111250 Moscow, Russia; art-marchenkov@yandex.ru (A.M.); bardakovvv@interunis-it.ru (V.B.); dariazhg@yandex.ru (D.Z.); karpova.m.v24@gmail.com (M.K.); timon.ba@mail.ru (T.B.)
[2] LLC INTERUNIS-IT, 111024 Moscow, Russia; serg@interunis-it.ru
* Correspondence: vera.barat@mail.ru

Abstract: In this study, we investigated defect detection in dissimilar welded joints by the acoustic emission (AE) method. The study objects were carbide and decarburized interlayers, which are formed at the fusion boundary between austenitic and pearlitic steels. Diffusion interlayers, as a structural defect, usually have microscopic dimensions and cannot be detected using conventional non-destructive testing (NDT) methods. In this regard, the AE method is a promising approach to diagnose metal objects with a complex structure and to detect microscopic defects. In this paper, the AE signatures obtained from testing defect-free specimens and specimens with diffusion interlayers are analyzed. We found that the AE signature for defective and defect-free welded joints has significant differences, which makes it possible to identify descriptors corresponding to the presence of diffusion interlayers in dissimilar welded joints.

Keywords: dissimilar welded joints; acoustic emission; defects; cyclic loading; NDT; pearlitic steel; austenitic steel; lack of penetration

Citation: Barat, V.; Marchenkov, A.; Bardakov, V.; Zhgut, D.; Karpova, M.; Balandin, T.; Elizarov, S. Assessment of the Structural State of Dissimilar Welded Joints by the Acoustic Emission Method. *Appl. Sci.* **2022**, *12*, 7213. https://doi.org/10.3390/app12147213

Academic Editor: Giuseppe Lacidogna

Received: 12 June 2022
Accepted: 16 July 2022
Published: 18 July 2022

1. Introduction

Heterogeneous welded joints are widely used in industry to optimize application and engineering requirements with economic considerations. For instance, dissimilar welding is frequently applied for the joining of pipelines at thermal and nuclear power plants, assemblies of steam and gas turbines, as well as technological pipelines at chemical and petrochemical enterprises. This technology can significantly reduce the material costs and the weight of the construction. However, the majority of dissimilar welded joints have complex microstructure due to the differences in mechanical, chemical and thermophysical properties of the welding materials. Moreover, there is a high level of residual stresses in such joints, which cannot be removed by post-weld heat treatment (PWHT). The complex structural and mechanical states of the welds interfere with the detection of defects and discontinuities when using conventional physical methods of control. As a result, dissimilar welded joints become a difficult object for diagnostics.

Besides typical defects such as cracks, undercuts and lack of penetration, the formation of specific defects also can be observed. In most cases, they may be associated with an abrupt change in the structure between the weld metal and the heat-affected zone in dissimilar welded joints. When dissimilar joints are obtained by fusion welding, diffusion zones are formed near the fusion lines. If the welded joint is made from steels of different structural classes, then the process of carbon diffusion will take place. In this case, decarburized interlayers and layers with a high content of carbides (carbide interlayers) are often located in welded joints [1,2]. If such dissimilar welded joints are operated for a long time at elevated temperatures, diffusion processes will proceed intensively throughout the entire service life. This will lead to the constant increase in interlayer size. The presence of such large interlayers will negatively affect the mechanical properties of the welded joints [3–5].

As a rule, a decarburized interlayer, the size of which can reach several millimeters, has a ferritic structure and low strength characteristics—ultimate tensile strength (UTS) and yield strength (YS). The presence of a hard carbide layer commonly increases the risk of sudden failure due to the great brittleness. Therefore, when conducting a non-destructive test of a joint, it is important to identify both structural defects and also zones with a sharp gradient in structure/chemical composition, e.g., diffusion interlayers [6].

Conventional NDT methods do not provide required sensitivity when testing dissimilar welded joints due to pronounced heterogeneity and anisotropy of the physical properties. The most sensitive method is ultrasonic testing. The use of ultrasonic testing for dissimilar welded joints of reactor equipment is noted in several works [7,8].Essentially, testing is carried out using special equipment and techniques that take into account the design features of each welded joint [9,10]. However, the coarse-grained structure leads to a high attenuation of ultrasonic vibrations in the austenitic steels, and the complex structure of a dissimilar welded joint displays a high level of interference [11]. Even though ultrasonic testing provides a fairly reliable detection of cracks, pores, cavities and lack of penetration, its sensitivity is not enough to detect structural defects, such as carbide and decarburized interlayers.

In this paper, we present information about the acoustic emission (AE) method application for diagnosing dissimilar welded joints of steels from different structural classes. The AE method is based on acoustic elastic wave generation when a material undergoes structural changes, for example, because of crack formation. The AE method is highly responsive to defect detection and can be applied to determine defect growth. Moreover, the AE method does not require a probing action, which allows it to be effectively used in structure health monitoring systems for loaded structures in the operating environment [12]. The use of the AE testing method for diagnostics of dissimilar welded joints is insufficiently studied nowadays. Few studies are devoted to the application of AE directly in the process of dissimilar welding [13–16] and only few experiences have been successful. In [17], the authors monitored the development of a crack in a dissimilar welded joint made of low-alloy pearlitic and austenitic steels. The study was carried out under laboratory conditions for a pre-hydrogenated specimen. The AE method showed high sensitivity since it was able to detect a crack with an opening of no more than 50 μm.

The high sensitivity of the AE testing method to the microstructure parameters reveals a great variety of changes in the material structure and composition. For example, in [18,19], the authors implemented AE to identify such microscopic AE sources as the destruction of carbide particles in high-strength steels. In [20], the authors studied martensitic transformations in steel with an austenitic structure, AISI 304. The influence of microstructure parameters of the parent metal and the weld metal was analyzed in [21] using the example of low-alloy pearlitic steel. The authors investigated the impact of the grain size, structural composition and the presence of non-metallic inclusions on the AE parameters and mechanical properties of the welded joint.

We studied the dissimilar welded joints of 12Kh18N10T austenitic steel to 09G2S pearlitic steel. In [22], AE monitoring under static tension of the dissimilar welded joint is investigated by the authors. Therefore, this research is devoted to the study of AE technique application under cyclic loading of dissimilar welded joints. The main goal of this work was to analyze the possibility of detecting diffusion decarburized and carbide interlayers based on AE data. The specimens of dissimilar welded joints with and without diffusion interlayers were tested using the AE method. The AE signature was analyzed at various stress values for defect-free specimens; some patterns of AE data were determined, indicating diffusion interlayers in the welded joints.

2. Materials and Methods

In this study, heterogeneous welded joints of 09G2S (pearlitic class) and 12Kh18N10T (austenitic class) steels were used. To produce welded joints, pairs of plates made of 09G2S and 12Kh18N10T steels with dimensions of 250 mm × 300 mm × 3 mm each were welded together by argon arc welding with a non-consumable electrode Sabaros SW146 filler wire with a diameter of 1.2 mm. The chemical composition of these steels and a filler material is presented in Table 1; the mechanical properties, determined by tensile tests, can be found in Table 2.

Table 1. Chemical composition of welded steels and a filler wire, wt %.

	12Kh18N10T Steel	09G2S Steel	Sabaros SW146 Wire (Reference Values)
C	<0.12	<0.12	0.10
Si	<0.8	0.5–0.8	0.80
Mn	<2	1.3–1.7	8.5
Ni	9–11	<0.3	8.5
S	<0.02	<0.04	–
P	<0.035	<0.035	–
Cr	17–19	<0.3	18.5
Cu	<0.3	<0.3	–
Ti	0.4–1	–	–
Fe	~67	balance	balance

Table 2. Mechanical properties of welded steels and the filler wire.

	12Kh18N10 Steel	09G2S Steel	Sabaros SW146 Wire (Reference Values)
Yield stress σ_y, MPa	270	390	>370
Ultimate tensile stress σ_u, MPa	550	520	>600
Uniform elongation δ_u, %	50	15	-
Total elongation δ, %	55	20	>35

To make a defect-free welded joint, welding of the plates was carried out in compliance with the recommended arc welding technology parameters. As a result, a welded joint with full penetration and austenitic structure of the weld metal was obtained (Figure 1a). No diffusion interlayers were observed near the fusion lines (Figure 1b). The structure of 09G2S steel near the fusion line was pearlitic, while the weld metal was austenitic.

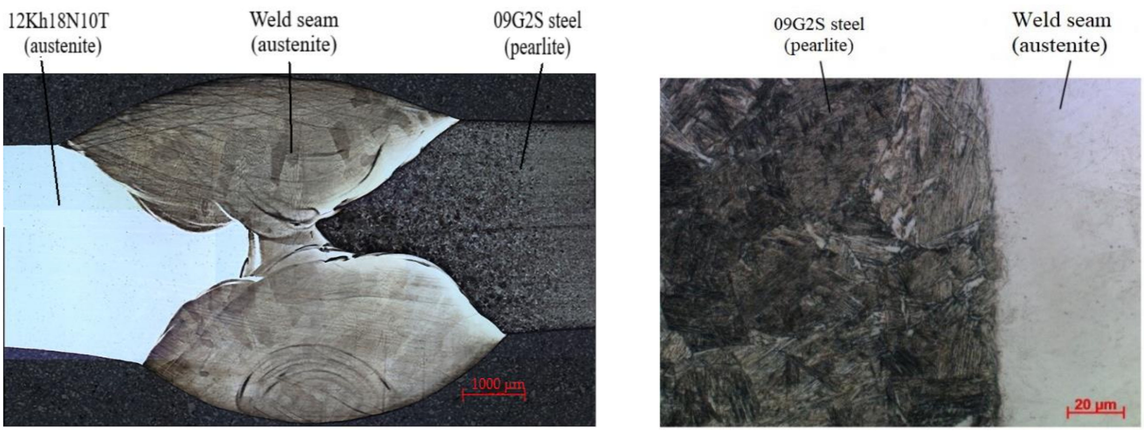

(**a**) (**b**)

Figure 1. Welded joint of steel 09G2S and 12Kh18N10T (**a**) and fusion line from the side of the steel 09G2S (**b**).

To obtain diffusion interlayers, some welded joints were submitted to post-weld heat treatment in Nabertherm P180 furnaces according to the following regime: heating to 650 °C and holding for 5 h and still air cooling. This heat treatment simulated long-term operation of these welded joints at high temperatures. Due to the presence of chromium and manganese in the composition of the SW146 filler wire, diffusion layers were formed in the near-weld zone. The structure of the heat-treated welded joint is shown in Figure 2.

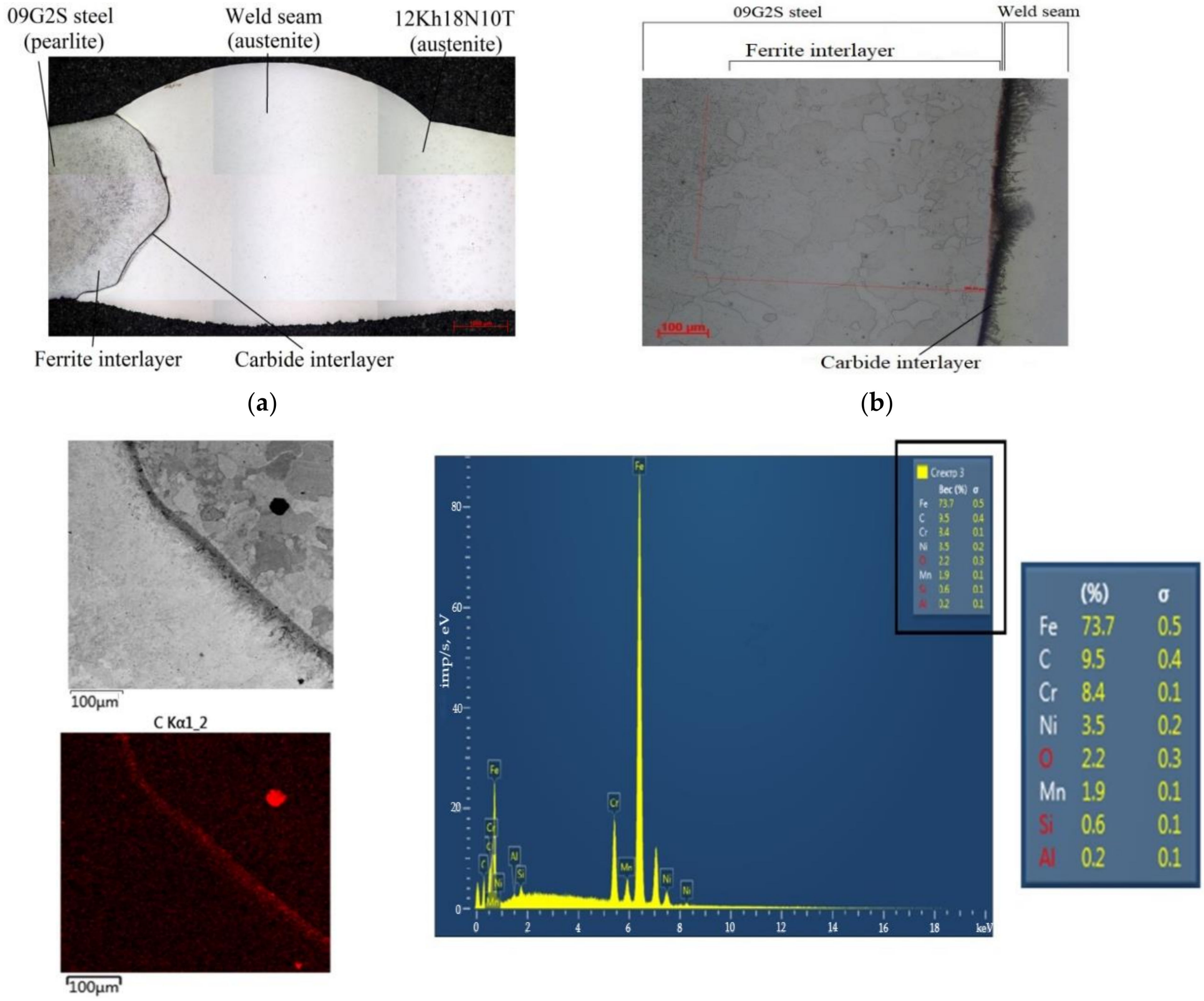

Figure 2. Welded joint of 09G2S and 12Kh18N10T steels after PWHT: weld (**a**) and cross-section of the fusion line from the side of 09G2S steel (**b**); SEM images (**c**) and EDX analysis results (**d**) of carbide interlayer.

Due to the carbon diffusion from 09G2S steel into the fusion line zone, a decarburized layer with a ferritic structure was formed. The thickness of such an interlayer was 500–700 µm (Figure 2b). In addition, near the fusion line on the side from the weld, a carbide interlayer formed due to the carbon diffusion into the weld. The thickness of the carbide layer was 10–70 µm, and 30 µm on average (see Figure 2b). Figure 2c shows a photo of the fusion line from the side of steel 09G2S, the distribution of carbon in this area and the chemical composition of the carbide interlayer, obtained by scanning electron microscopy (SEM) and energy-dispersive X-ray spectroscopy (EDX). The results indicate high carbon content in the interlayer formed as a result of carbon diffusion during additional heat treatment.

Flat specimens were made for mechanical testing with a width of the gauge section of 20 mm from the obtained welded joints. Tensile tests were carried out on an Instron 5982 testing machine with a constant crosshead speed of 2 mm/min. Cyclic tensile tests were carried out on an Instron 8801 testing machine; loading parameters were set as sinusoidal tensile cycles with a frequency of 1 Hz and a cycle load ratio R = 0.05; the value of the maximum cycle stress σ_{max} varied from 200 to 400 MPa based on the specimen type. A total of 18 specimens were studied: 9 specimens without PWHT (without interlayers) and 9 specimens after PWHT (with interlayers).

AE data were recorded using the A-Line 32 system («INTERUNIS-IT», LLC, Moscow, Russia). Four AE sensors were fixed on each specimen. Two of them were located at the edges of the gauge section and the other two limited the weld metal zone. The design of the test specimen with the designation of the AE sensors location is shown in Figure 3. The measurement of acoustic path was performed by GT200 resonant sensors (GlobalTest, LLC, Moscow, Russia) with a resonant frequency of 180 kHz and PAEF-014 electrical signal preamplifiers. The noise of the equipment, preamplifier and AE sensors amounted to 26 dB. A digital filter with a bandwidth of 100–400 kHz was used to suppress the noise of the testing machine during data collection. The threshold for acoustic signals discrimination was set to 50 dB. The value of the dead time was chosen as the minimum possible, 32 μs, so as not to affect the measurement results.

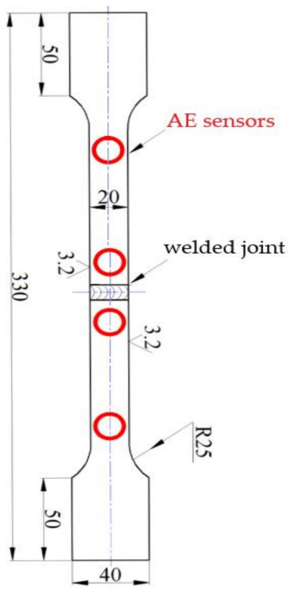

(**a**)

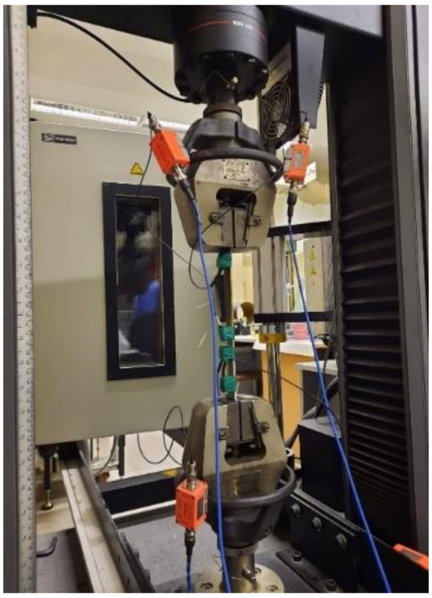

(**b**)

Figure 3. The design of the test specimen (**a**) and the experimental installation photo (**b**).

3. Results

It is advisable to start with considering patterns of AE data recorded under static loading (described in detail in [22]) to gain deep knowledge and understanding of AE data parameters under cyclic loading. Figure 4 shows the AE data obtained under static tension of a specimen without interlayers. There are two pronounced maxima: the first approximately corresponds to the yield strength of 12Kh18N10T steel (stress is about 250–300 MPa); the second one is achieved at the stress level which corresponds to the yield stress of 09G2S steel (about 400 MPa).

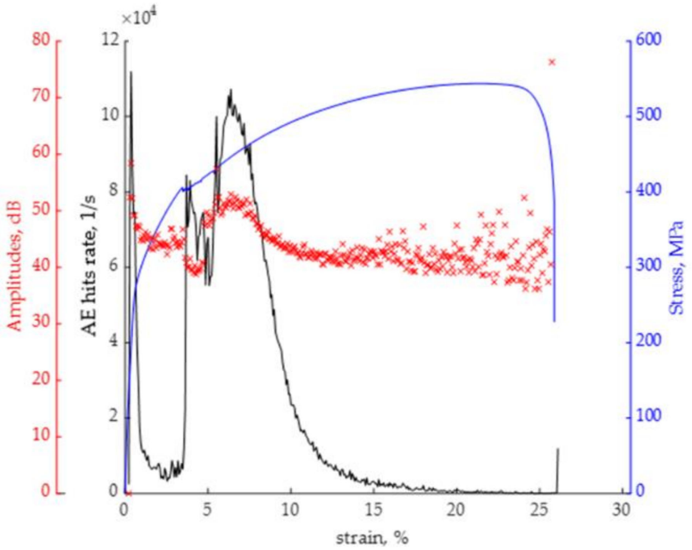

Figure 4. AE data recorded under tension of a specimen with a dissimilar welded joint of 12Kh18N10T to 09G2S steels without diffusion interlayers. All three data arrays (stress—blue, AE hits rate—black, and AE amplitude—red) depend on the same argument (strain, %).

Based on this information, tests with maximum cycle stresses σ_{max} = 200, 300 and 400 MPa are of greatest interest. The stress of 200 MPa is close to the maximum allowable stress (only elastic deformation), and 300 and 400 MPa stress levels cause the start of plastic deformation. These values correspond to the yield strength of 12Kh18N10T and 09G2S steels, respectively. Figure 5a,b show AE data obtained under cyclic loading of a dissimilar welded joint without diffusion interlayers at σ_{max} = 200 MPa. Figure 5a shows AE hit amplitudes and AE hit rate, and Figure 5b reveals the result of AE event location. Since at σ_{max} = 200 MPa, the deformation has been predominantly elastic, AE generation was not very active. No more than 1–2 AE hits were recorded per one loading cycle. The average activity was 0.05 AE hits per cycle, and the AE hit amplitudes did not exceed 65 dB. The location of AE events occurred non-intensively and almost evenly over the surface of the specimen.

At the maximum stress σ_{max} = 300 MPa (Figure 5c,d), AE hits were generated more actively, the average activity value was 0.2 AE hits per cycle, the overall amplitude level increased and high-amplitude AE hits with an amplitude of 70–75 dB appeared. AE event location was determined outside the welded joint in the base metal, 12Kh18N10T steel. At the maximum stress σ_{max} = 400 MPa (Figure 5e,f), the generation of AE hits was quite active, and the AE hit rate reached 6–8 hits per cycle, with AE events located mainly outside the welded joint in the base metal, 09G2S.

To identify some failure predictors of a dissimilar welded joint, it is informative to represent AE data using a scatterplot. One axis plots the rise time of the AE hit, and the other axis shows its amplitude (Figure 6).

The scatter with the value of σ_{max} = 200 MPa in the absence of possible AE sources is a cloud of randomly scattered points; at σ_{max} = 300 MPa corresponding to the plastic deformation of 12Kh18H10T steel, an ordered arrangement of indications on the scatterplot is observed, and AE hits are grouped into horizontal chains (selected regions in Figure 6b). Groups of AE hits have different amplitudes, but their rise time values are close to each other. At σ_{max} = 400 MPa, when plastic deformation of 09G2S steel occurred, many points are displayed on the scatterplot, and many horizontal oriented zones are formed.

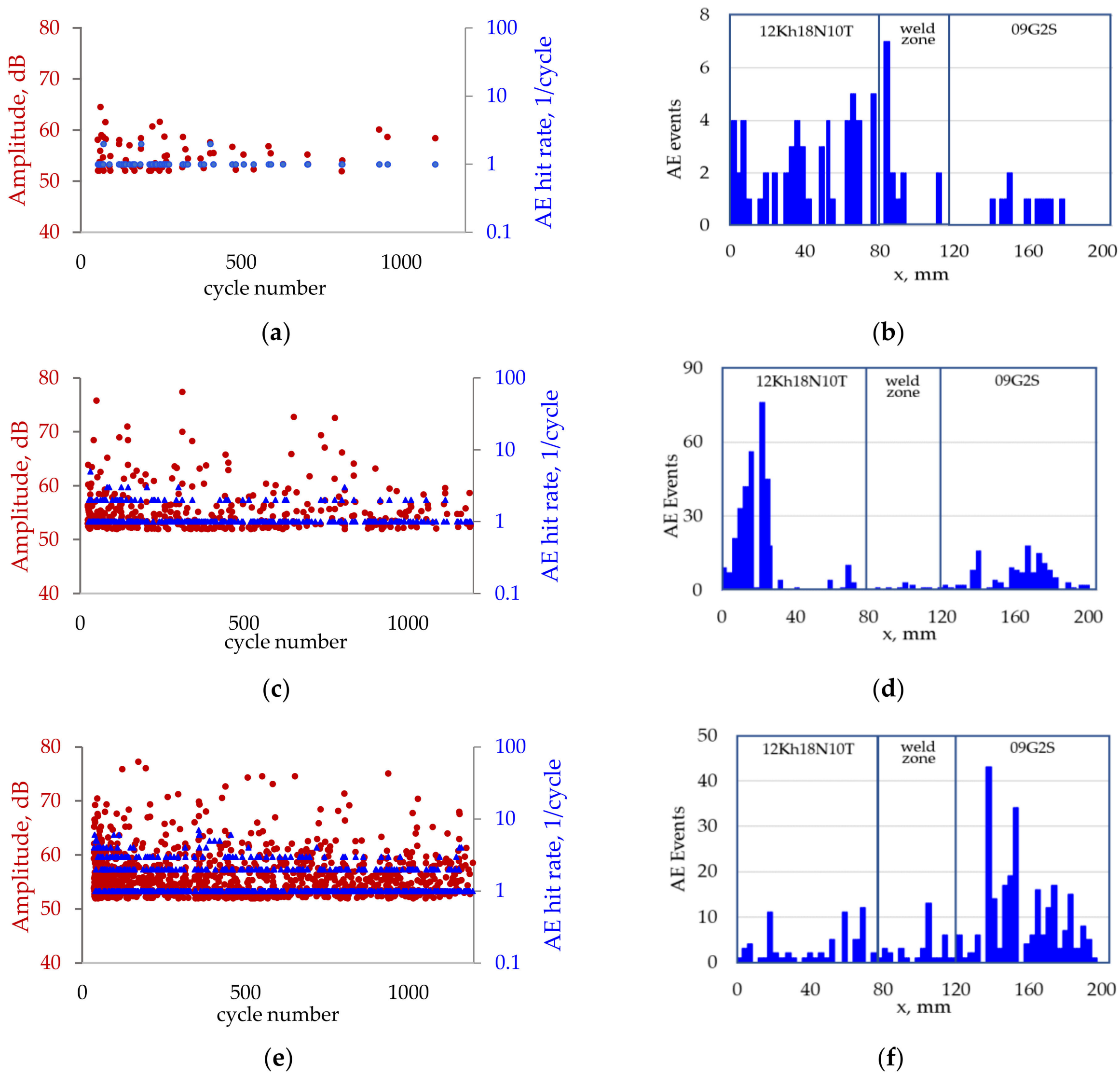

Figure 5. AE data obtained during cyclic loading of a welded joint without diffusion interlayers. Location of AE events at σmax = 200 MPa (**a**), σmax = 300 MPa (**c**), σmax = 400 MPa (**e**); AE hit count rate values at σmax = 200 MPa (**b**), σmax = 300 MPa (**d**) and σmax = 400 MPa (**f**).

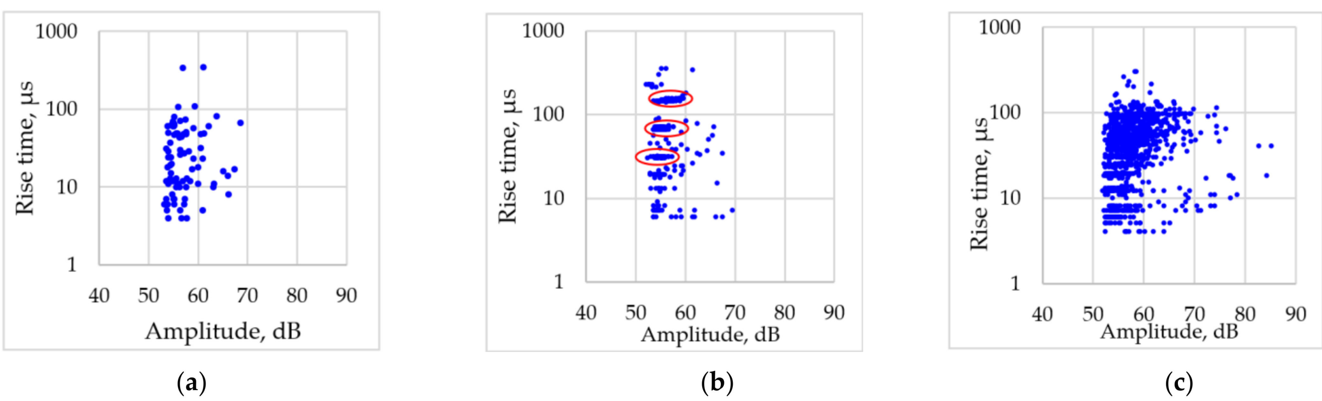

Figure 6. Rise time vs. amplitude scatterplots for AE hits registered under cyclic loading of a defect-free welded joint at σ_{max} = 200 MPa (**a**), σ_{max} = 300 MPa (**b**) and σ_{max} = 400 MPa (**c**).

A cluster analysis was performed for a more detailed study of the AE data. AE signals were combined into clusters based on the waveform similarity. The cross-correlation coefficient was used as a distance measure. As a result of cluster analysis, it was found that the AE hits that were grouped into horizontal chains had a similar shape and are correlated with a cross-correlation coefficient r = 0.65–0.8. A representative cluster was formed with a specific signal waveform for the data obtained under cyclic loading with cycle amplitude of 300 MPa, as in Figure 6a. The quantity of AE hits in the cluster was approximately 10% of the total number of registered AE hits. The quantity of correlated signals increases with increasing load. The quantity of correlated signals at σ_{max} = 400 MPa increased to 20%. One of the typical AE signal shapes is shown in Figure 7b.

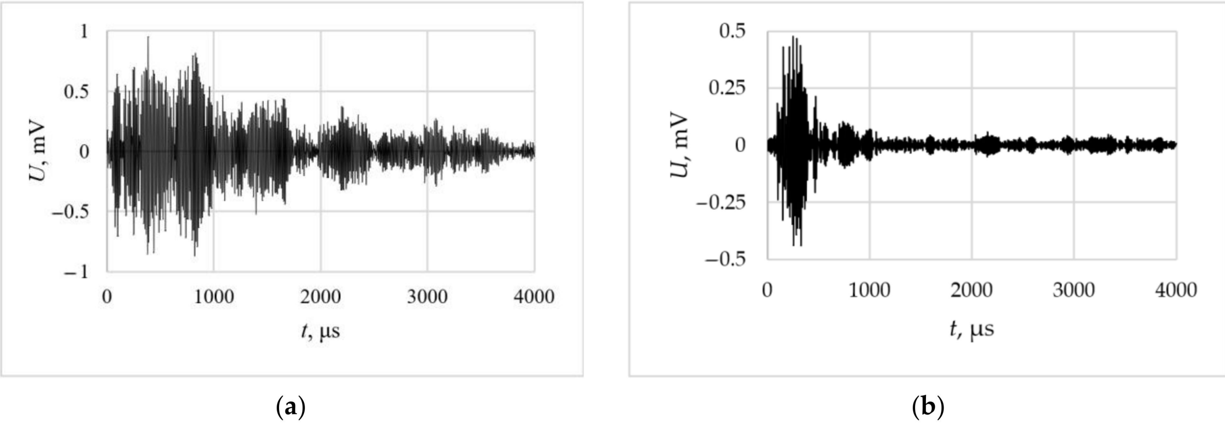

Figure 7. Typical AE signal waveforms for defect-free specimen at σ_{max} = 300 MPa (**a**) and σ_{max} = 400 MPa (**b**).

AE data recorded when testing dissimilar welded joints specimens with diffusion interlayers had some peculiarities in comparison with the AE data described earlier. Figure 8 shows the data obtained during the tension test of a specimen with diffusion interlayers. An additional maximum was observed at the stress range of 250–300 MPa. It belongs to the ultimate tensile stress of the ferritic structure. Therefore, it can be assumed that the additional maximum of the AE data is an indicator of a decarburized diffusion interlayer.

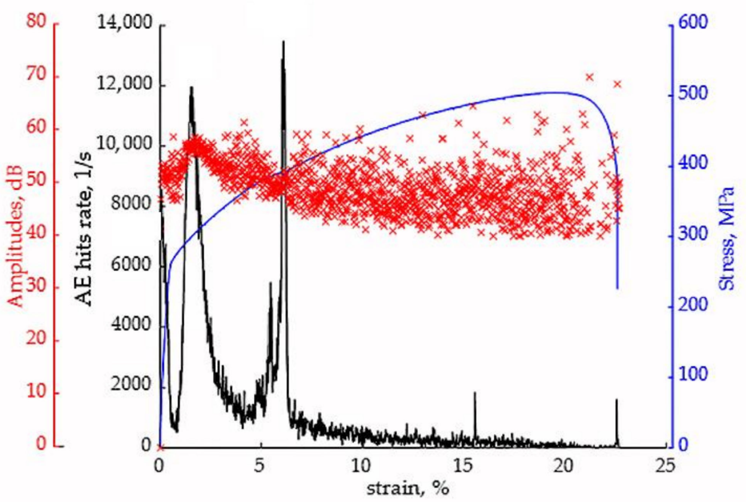

Figure 8. AE data recorded under tension of a specimen of a dissimilar welded joint with diffusion interlayers. All three data arrays (stress—blue, AE hits rate—black, and AE amplitude—red) depend on the same argument (strain, %).

Figure 9 shows AE hit amplitude, AE hit rate and AE event location results when loading a dissimilar welded joint with diffusion interlayers with sinusoidal cyclic stress with maximum stresses σ_{max} = 200, 300 and 400 MPa. The AE data obtained under cyclic loading of a specimen with carbide and decarburized interlayers differs significantly from the AE data recorded when loading a defect-free specimen (Figure 5). The difference is clearly demonstrated at low maximum stresses. Thus, at σ_{max} = 200 MPa (Figure 9a), the AE hit rate sometimes exceeds 5 AE hits per cycle, and the average value is 0.95 AE hits per cycle, which is about 20 times higher than for a defect-free specimen. At the weld zone (Figure 9b), there is a cluster which suggests that the source of AE is the weld zone itself at a given loading level.

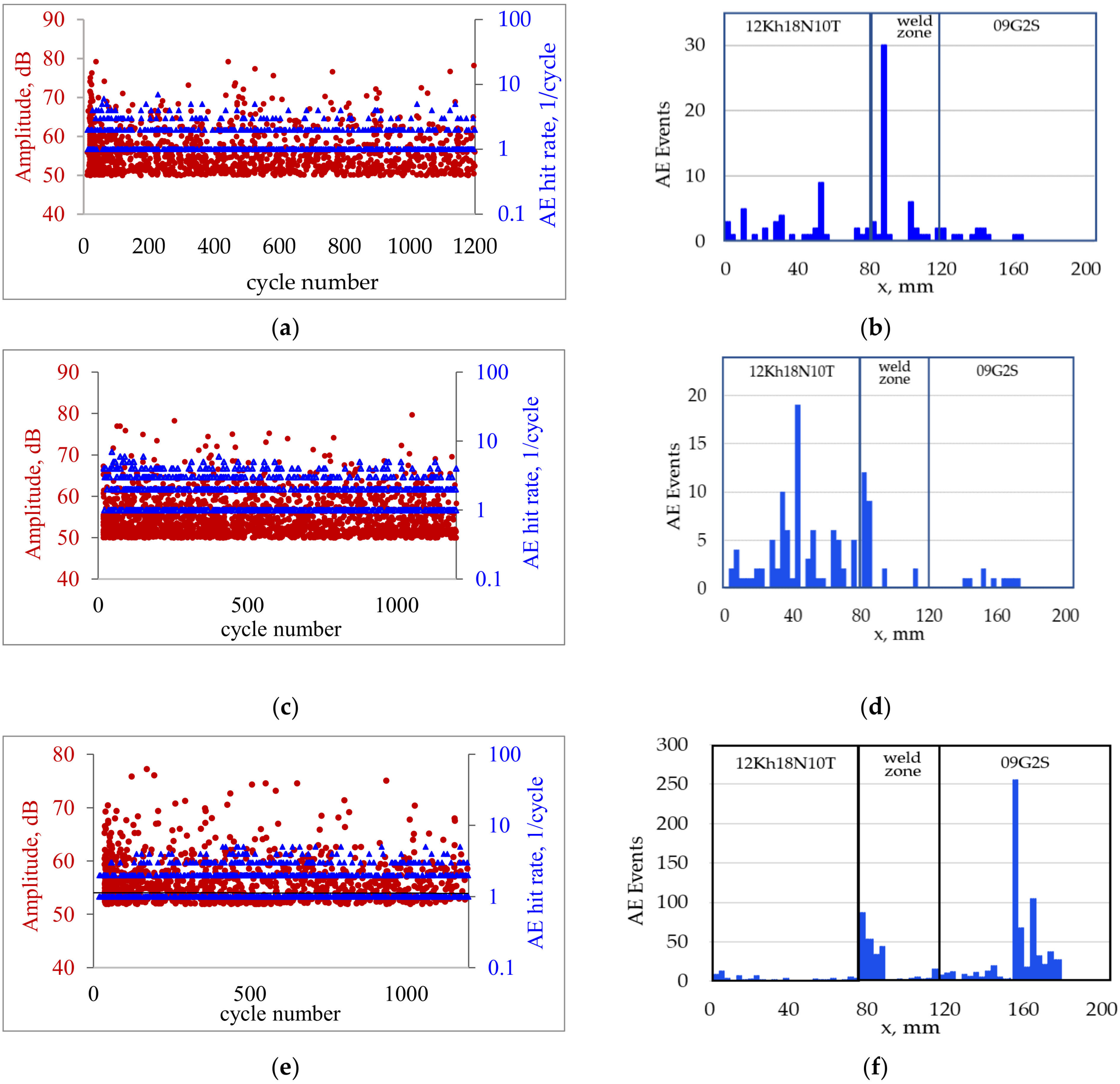

Figure 9. AE data obtained during cyclic loading of a welded joint with diffusion interlayers. Location of AE events at σ_{max} = 200 MPa (**a**), σ_{max} = 300 MPa (**c**) and σ_{max} = 400 MPa (**e**); AE hits count rate values at σ_{max} = 200 MPa (**b**), σ_{max} = 300 MPa (**d**) and σ_{max} = 400 MPa (**f**).

At a maximum stress of 300 MPa (Figure 9c,d), the AE hit rate increases, the average value is 1.5 hits/cycle, the amplitudes of the AE hits reach 70–80 dB and the location of AE events is observed not only in the weld zone, but also in the base metal, 12Kh18N10T steel. With a growth of the maximum stress to 400 MPa (Figure 9e,f), the level of AE hit rate decreases, and its average value is 1.1 AE hits per cycle; the location of AE events occurs mainly in the region of 09G2S steel.

The difference between the AE hits parameters recorded during loading of a defect-free and a defective welded joint is clearly shown in the rise time vs. amplitude scatterplots (Figure 10). Representation of the data in the form of a scatterplot makes it possible to determine that the increase in AE hit rate occurs due to the appearance of a group of AE hits with similar rise times, which leads to a significant change in the form of the scatterplot. The scatterplot for a defect-free specimen at σ_{max} = 200 MPa (Figure 6a) displays a cloud of low-density, randomly scattered points. At the same time, a horizontally oriented cluster is distinguished in the lower part of the scattering diagram for a specimen with diffusion interlayers (Figure 10a). This region is formed by AE hits of different amplitudes, but with similar and low rise time values (marked with a red ellipse). In the scatterplot with σ_{max} = 300 MPa (Figure 10b), a similar region is also presented. It contains a larger number of indications and combines more AE hits. At σ_{max} = 400 MPa, the scattering diagram (Figure 10c) displays more points, just as in the defect-free case. Many horizontally oriented groups of indications are formed.

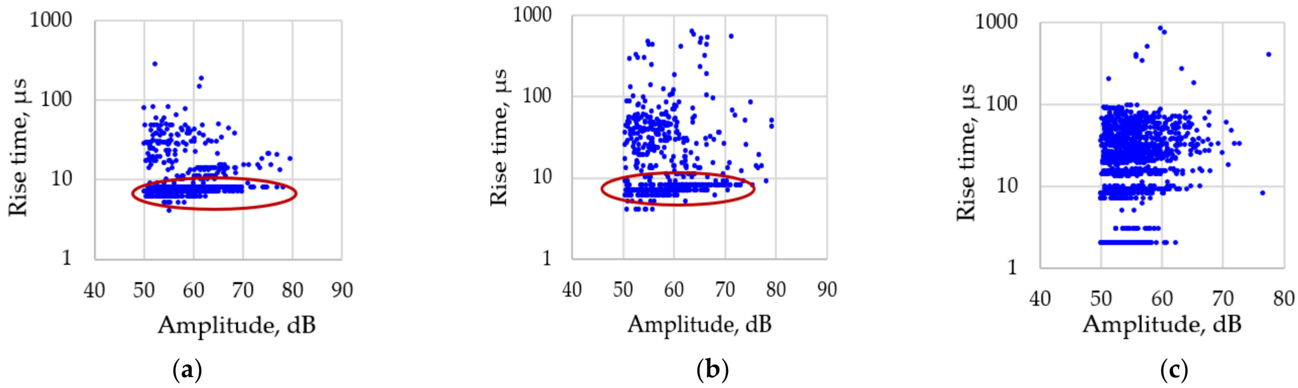

Figure 10. Rise time vs. amplitude scatterplots for AE hits registered under cyclic loading of a specimen with diffusion layers at σ_{max} = 200 MPa (**a**) σ_{max} = 300 MPa (**b**) and σ_{max} = 400 MPa (**c**).

Figure 11 shows the frequency histogram of the AE hits' rise times obtained at σ_{max} = 200 MPa. This histogram can be considered as an empirical distribution of the rise time parameter. In Figure 11a, corresponding to a defect-free welded joint, the rise time distribution is close to uniform, and in Figure 11b, corresponding to a welded joint with diffusion interlayers, we can see a single mode with a high frequency of observations.

For AE signals obtained during loading of a dissimilar welded joint with diffusion interlayers, cluster analysis was performed using the same method as for a defect-free specimen. It was found that AE hits with equal rise time are grouped in a scatterplot into horizontally oriented regions (marked with a red ellipse in the Figure 9a,b). All of them have a similar waveform and correlate with r = 0.7–0.9. Figure 12 shows the signals corresponding to weld deformation at stress σ_{max} = 200 MPa (Figure 12a) and σ_{max} = 300 MPa (Figure 12b). As can be seen, the AE signals have the same waveform and characterize practically identical physical processes.

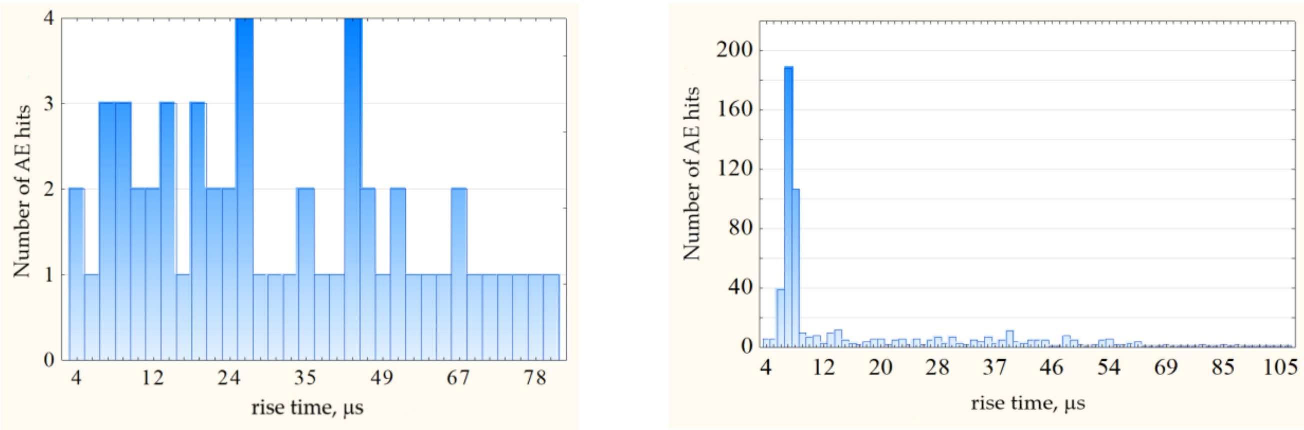

(a) (b)

Figure 11. Frequency histogram of AE hits' rise times for defect-free welded joint (**a**) and for welded joint with diffusion interlayers (**b**).

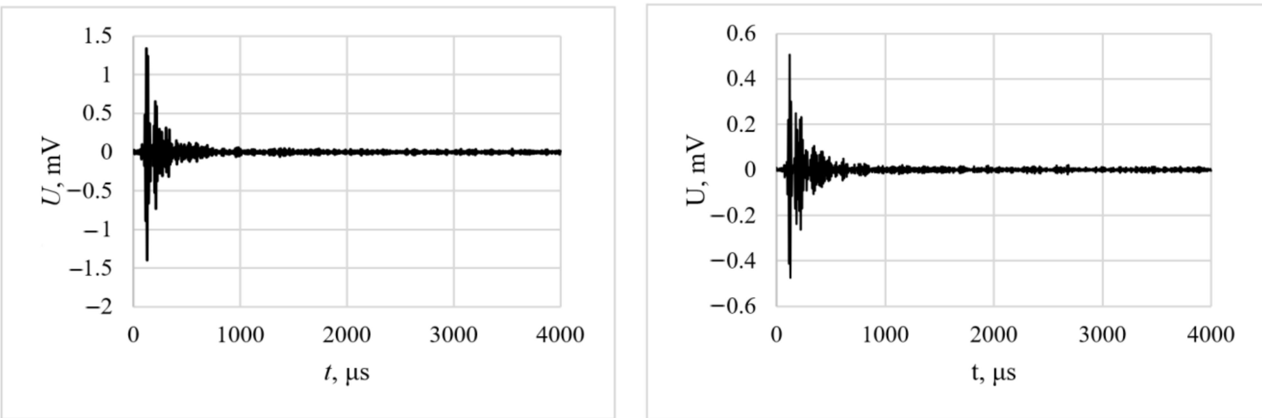

(a) (b)

Figure 12. Typical AE signal waveforms of a specimen with diffusion layers at σ_{max} = 300 MPa (**a**) and σ_{max} = 400 MPa (**b**).

4. Discussion

Features of AE data during the cyclic loading of dissimilar welded joints without diffusion interlayers, as well as during static tension, correspond to the inhomogeneous nature of the object under study. At stress σ_{max} equal to 200 MPa, the weld and base metal experience elastic deformation (Figure 4). AE hit generation in this case is non-intense; the average AE hit rate is 0.05 AE hits per cycle. This can be explained by the small number of mobile dislocations, which are sources of AE, as well as the absence of material structural elements that can cause failure at a given stress. The obtained result fits the theory of AE [23] and does not contradict the fundamental studies [16]. A more detailed analysis of the AE data showed that the parameters of the AE hits, such as the amplitude and rise time, are mostly random and have a considerable scatter of values (Figure 6a). The lack of ordering parameters indicates the scattered nature of the destruction [24,25].

The load range σ_{max} = 250–300 MPa corresponds to the beginning of plastic deformation of steel 12Kh18N10T, which is manifested by more intense AE generation with the appearance of high-amplitude AE hits up to 80 dB. The correspondence of the AE data to the process of plastic deformation of austenitic steel is confirmed by the location results (Figure 5d), i.e., the indications of AE events located in the parent metal area from the side of steel 12Kh18N10T. The scatterplot (rise time vs. amplitude) at σ_{max} = 300 MPa acquires an ordered form due to the grouping of indications into horizontal lines corresponding to

AE hits with different amplitudes, but equal rise time values. AE hit rise time depends both on the type of AE source and its location; therefore, AE hits with the same rise time are most likely emitted by the same localized AE source. Analysis of the AE signals waveform showed that the AE signals belonging to the same cluster on the scatterplot have a similar waveform, with a cross-correlation coefficient of 0.6–0.8. A typical AE signal waveform is shown in Figure 7. The burst nature of this signal, relatively high amplitude and a specific waveform make it possible to assume that the process of twinning during plastic deformation of austenitic steel was recorded [26].

AE activity increases and the AE source position occurs over the entire surface of the specimen with predominant localization in the parent metal from the side of 09G2S steel when the maximum stress is 400 MPa. The scatterplot (Figure 6c) for a given stress value is a set of horizontal lines of AE hits with equal rise times. The results of cluster analysis of AE signals show the presence of many AE signals with similar waveforms. This AE signature can be explained by the several active AE sources and characterizes the process of plastic deformation of the parent steel 09G2S.

Tests of specimens of dissimilar welds with diffusion interlayers have shown that the presence of carbide and decarburized interlayers can be determined based on AE data. Thus, at close to operational stress σ_{max} = 200 MPa, AE hit generation is 20 times more active, and the average value of the AE hit rate turns out to be 20 times higher than for defect-free specimens (Figure 9a). The results of cluster analysis showed that an increase in AE hit rate occurs due to the generation of AE hits of similar waveform (Figure 12); in this case, a cluster is formed on the rise time vs. amplitude scatterplot and a distribution of rise time acquires some specific changes, indicating the presence of diffusion interlayers.

There are at least three reasons why these AE signals can be associated with the presence of diffusion layers in the dissimilar welded joint. Firstly, these AE signals waveforms are specific for specimens with diffusion interlayers; when testing defect-free welded joints, signals of this waveform were not recorded. Secondly, signals of a specific waveform appear at a stress of 250–300 MPa. This level of stress equals the ultimate tensile stress of the ferrite phase. Moreover, an additional maximum of the AE hit rate appeared in the specimen with interlayers under static tension at such loads. In addition, such an AE waveform was detected during tension of dissimilar welded joints with diffusion interlayers in [22].

Based on highly mentioned reasons, it can be concluded that AE signals with a repeated waveform with different amplitudes and low AE rise time (up to 10 μs) are markers of diffusion layers presence in a dissimilar welded joint.

5. Conclusions

This results of this study illustrate the possibility of using the AE method to detect diffusion interlayers in dissimilar welded joints of pearlitic and austenitic steels. Diffusion interlayers, including carbon and diffusion interlayers, are specific structural defects, the presence of which can adversely affect the mechanical properties of welded joints. Diffusion interlayers are usually microscopic in size and cannot be detected by conventional non-destructive testing (NDT) methods. Therefore, the possibility of using AE testing to detect diffusion interlayers is of great importance for practical applications.

As a result of this research, we found that diffusion interlayers under cyclic loading are an active source of AE and emit acoustic signals of a similar specific waveform. Therefore, the presence of diffusion interlayers can be detected not only by an increase in the frequency of AE hits, but also by the presence of such deterministic ordered signals with a certain waveform. These signals can be detected using cluster analysis or by a rise time parameter that is constant for signals of similar waveform. The appearance of AE hits set with the same rise time leads to structuring of scattering diagrams (rise time vs. amplitude) and a change in the AE hits' rise time distribution. The reliability of diffusion interlayers detection is confirmed by the AE event location distributions—the AE source is detected in the area of a dissimilar welded joint.

The results obtained can be used to determine the diagnostic criteria for the detection of defects and the subsequent development of an industrial NDT technique for dissimilar welded joints.

Author Contributions: Conceptualization, V.B. (Vera Barat) and A.M.; methodology, V.B. (Vera Barat); software, M.K.; validation, V.B. (Vladimir Bardakov) and T.B.; formal analysis, M.K.; investigation, V.B. and A.M.; resources, S.E.; data curation, T.B. and D.Z.; writing—original draft preparation, V.B. (Vera Barat); writing—review and editing, V.B. (Vladimir Bardakov); visualization, D.Z.; supervision, S.E.; project administration, S.E. and A.M. All authors have read and agreed to the published version of the manuscript.

Funding: The research was carried out within the framework of the project "Diagnostics of dissimilar welded joints of pearlitic and austenitic steels by the acoustic emission" with the support of a grant from NRU "MPEI" for the implementation of scientific research programs "Energy", "Electronics, Radio Engineering and IT", and "Industry 4.0, Technologies for Industry and Robotics" in 2020–2022 (project no. 20/22-0000028/44).

Institutional Review Board Statement: Not applicable.

Informed Consent Statement: Not applicable.

Data Availability Statement: Not applicable.

Conflicts of Interest: The authors declare no conflict of interest.

References

1. Saini, M.; Arora, N.; Pandey, C.; Mehdi, H. Mechanical properties of bimetallic weld joint between SA 516 grade 65 carbon steel and SS 304 L for steam generator application. *Int. J. Res. Eng. Technol.* **2014**, *3*, 39–42. [CrossRef]
2. Goncharov, A.L.; Marchenkov, A.Y.; Terentyev, E.V.; Zhmurko, I.E.; Sliva, A.P. Study of structural non-homogeneity impact on mechanical properties of dissimilar weld joints of carbon steel 20 and corrosion-resistant austenitic 12Kh18N10T steel. *IOP Conf. Ser. Mater. Sci. Eng.* **2019**, *681*, 012016. [CrossRef]
3. Sharma, P.; Dheerendra, K.D. A-TIG welding of dissimilar P92 steel and 304H austenitic stainless steel: Mechanisms, microstructure and mechanical properties. *J. Manuf. Processes* **2019**, *44*, 166–178. [CrossRef]
4. Suwannatee, N.; Wonthaisong, S.; Yamamoto, M.; Shinohara, S.; Phaoniam, R. Optimization of welding conditions for hot-wire GMAW with CO2 shielding on heavy-thick butt joint. *Weld. World* **2022**, *66*, 833–844. [CrossRef]
5. Margono, B.; Atmaja, H.I.; Wibowo, J.; Alfayed, A.; Rananto, R.F. Effect of pressure and welding time on physical and mechanical properties of dissimilar metal AISI 316 austenitic stainless steel and AISI 4140 alloy steel joints using friction welding. *Phys. Conf. Ser.* **2018**, *1517*, 1. [CrossRef]
6. Voiculescu, I.; Geanta, V.; Stefanescu, E.V.; Simion, G.; Scutelnicu, E. Effect of Diffusion on Dissimilar Welded Joint between Al0. 8CoCrFeNi High-Entropy Alloy and S235JR Structural Steel. *Metals* **2022**, *12*, 548. [CrossRef]
7. Hwang, Y.I.; Park, J.; Kim, H.J.; Song, S.J.; Cho, Y.S.; Kang, S.S. Performance Comparison of Ultrasonic Focusing Techniques for Phased Array Ultrasonic Inspection of Dissimilar Metal Welds. *Int. J. Precis. Eng. Manuf.* **2019**, *20*, 525–534. [CrossRef]
8. Gester, A.; Wagner, G.; Pöthig, P.; Bergmann, J.P.; Fritzsche, M. Analysis of the oscillation behavior during ultrasonic welding of EN AW-1070 wire strands and EN CW004A terminals. *Weld. World* **2022**, *66*, 567–576. [CrossRef]
9. Kumar, S.; Menaka, M.; Venkatraman, B. Performance comparison of phased array transducers for inspection of dissimilar welds on nuclear reactor components. *Ann. Nucl. Energy* **2021**, *162*, 108482. [CrossRef]
10. Dhayalan, R.; Kumar, A.; Mukhopadhyay, C.K. EMAT-Phased Array Inspection of Thick Austenitic Stainless Steel and Dissimilar Metal Welds. In *Lecture Notes in Mechanical Engineering*; Springer: Singapore, 2021; pp. 341–352. [CrossRef]
11. Da Cruz Payão Filho, J.; Passos, E.K.D.; Gonzaga, R.S.; Santos, D.D.; Maia, V.P.; Juliano, D.R. The influence of the welding process on the ultrasonic inspection of 9%Ni steel pipe circumferential welded joints. *Materials* **2020**, *13*, 961. [CrossRef]
12. Ono, K. Current understanding of mechanisms of acoustic emission. *J. Strain Anal. Eng. Des.* **2005**, *40*, 1–15. [CrossRef]
13. Ennaceur, C.; Beaugrand, V. Acoustic Emission Monitoring of Crack Growth in Dissimilar Joints for Corrosion Resistant Applications. In Proceedings of the 28th European Conference on Acoustic Emission Testing, Krakow, Poland, 17–19 September 2008; pp. 64–69.
14. Wuriti, G.S.; Chattopadhyaya, S.; Krolczyk, G. Comparison of Acoustic Emission Data Acquired During Tensile Deformation of Maraging Steel M250 Welded Specimens. *Arch. Acoust.* **2020**, *45*, 221–231. [CrossRef]
15. Vinogradov, A.Y.; Merson, D.L. The Nature of Acoustic Emission during Deformation Processes in Metallic Materials. *Low Temp. Phys.* **2018**, *44*, 930–937. [CrossRef]
16. Kumar, J.; Sarmah, R.; Ananthakrishna, G. General Framework for Acoustic Emission during Plastic Deformation. *Phys. Rev. B* **2015**, *92*, 144109. [CrossRef]

17. Builo, S.I. Diagnostics of the Predestruction State Based on Amplitude and Time Invariants of the Flow of Acoustic-Emission Acts. *Russ. J. Nondestruct. Test.* **2004**, *40*, 561–564. [CrossRef]
18. Restaged, I.; Danyuk, A.; Afanas'yev, M.; Merson, D.; Berto, F.; Vinogradov, A. Acoustic Emission Assessment of Impending Fracture in a Cyclically Loading Structural Steel. *Metals* **2016**, *6*, 266. [CrossRef]
19. Rastegaev, I.A.; Rastegaeva, I.I.; Merson, D.L.; Chugunov, A.V. Assessment of Conditions for Detecting Corrosion Cracking of Welded Joints by Acoustic Emission Method. *Chem. Pet. Eng.* **2020**, *56*, 554–562. [CrossRef]
20. Chen, G.; Luo, H.; Yang, H.; Han, Z.; Lin, Z.; Zhang, Z.; Su, Y. Effects of the welding inclusion and notch on the fracture behaviors of low-alloy steel. *J. Mater. Res. Technol.* **2019**, *8*, 447–456. [CrossRef]
21. Chai, M.; Qin, M.; Zheng, Y.; Hou, X.; Zhang, Z.; Cheng, G.; Duan, Q. Acoustic Emission Detection during Welding Residual Stresses Release in 2.25Cr1Mo0.25V Steel Welds. *Mater. Today Proc.* **2018**, *5*, 13759–13766. [CrossRef]
22. Barat, V.; Marchenkov, A.; Bardakov, V.; Karpova, M.; Zhgut, D.; Elizarov, S. Features of Acoustic Emission in Tensile Testing of Dissimilar Welded Joints of Pearlitic and Austenitic Steels. *Appl. Sci.* **2021**, *11*, 11892. [CrossRef]
23. Vinogradov, A.; Yasnikov, I.S.; Merson, D.L. Phenomenological approach towards modelling the acoustic emission due to plastic deformation in metals. *Scr. Mater.* **2019**, *170*, 172–176. [CrossRef]
24. McCrory, J.P.; Vinogradov, A.; Pearson, M.R.; Pullin, R.; Holford, K.M. Acoustic emission monitoring of metals. *Materials* **2022**, *15*, 328. [CrossRef]
25. Kuten, M.; Bobrov, A. Analysis of criteria for identification of defects by acoustic emission method. In *International Scientific Siberian Transport Forum TransSiberia 2021, Lecture Notes in Networks and Systems*; Springer: Cham, Switzerland, 2021; Volume 402. [CrossRef]
26. Vinogradov, A.; Orlov, D.; Danyuk, A.; Estrin, Y. Deformation mechanisms underlying tension-compression asymmetry in magnesium alloy ZK60 revealed by acoustic emission monitoring. *Mater. Sci. Eng. A* **2015**, *621*, 243–251. [CrossRef]